High-Temperature Majorana Corner States

Qiyue Wang,[1] Cheng-Cheng Liu,[2] Yuan-Ming Lu,[3] and Fan Zhang[1,*]
[1]Department of Physics, University of Texas at Dallas, Richardson, Texas 75080, USA
[2]School of Physics, Beijing Institute of Technology, Beijing 100081, China
[3]Department of Physics, Ohio State University, Columbus, Ohio 43210, USA

(Received 18 April 2018; revised manuscript received 26 September 2018; published 30 October 2018)

Majorana bound states often occur at the end of a 1D topological superconductor. Validated by a new bulk invariant and an intuitive edge argument, we show the emergence of one Majorana Kramers pair at each corner of a square-shaped 2D topological insulator proximitized by an $s_{\pm}$-wave (e.g., Fe-based) superconductor. We obtain a phase diagram that addresses the relaxation of crystal symmetry and edge orientation. We propose two experimental realizations in candidate materials. Our scheme offers a higher-order and higher-temperature route for exploring non-Abelian quasiparticles.

DOI: 10.1103/PhysRevLett.121.186801

Introduction.—A central theme in condensed matter physics is to discover and classify distinctive states of matter. Conventionally, states such as magnets or superconductors are characterized by the time-reversal or gauge symmetry that they spontaneously break. Over the last decade, the discovery of topological insulators (TIs) has opened the door to various classes of topological states of matter [1–4]. In each class, all of the states respect the same symmetries, yet they are indexed by the different values of a bulk topological invariant, which determine the physics on their boundaries of one dimension lower. As a prime example, for a 2D (3D) TI, the nontrivial $\mathbb{Z}_2$ index of the insulating bulk state dictates the presence of a gapless 1D (2D) edge (surface) state. When coupled to a magnet or superconductor that breaks an essential symmetry, the boundary state may acquire an energy gap and may even be passivated [5–8].

Recently, a novel class of TIs coined "higher-order TIs" [8–22] has emerged. They host protected gapless states on boundaries of more than one dimension lower. For instance, a second-order 2D (3D) TI has gapless corner (hinge) states between distinct edges (surfaces) that are gapped. While the emergent corner states have been realized in a phononic quadrupole TI [10], the prototype hinge states have been responsible for a quantum anomalous Hall effect [8]. These examples have enlightened the search for fascinating higher-order topological matter.

Meanwhile, *a priority* in condensed matter physics is to create topological superconductors (TSCs) with Majorana bound states, which offer a decoherence-free platform for quantum computing [23–26]. One route [27–41] is to employ an architecture that proximity couples an ordinary superconductor to a material that effectively has one helical band, which requires a magnetic field or a π Josephson junction. While experiments are achieving this goal [42–66], one might wonder whether there exists a new route: is there any higher-order TSC whose nontrivial bulk topology leads to the emergence of Majorana bound states? If the answer is in the affirmative, how can such a TSC be realized in an experimentally accessible setup?

Here we show that a second-order TSC in class DIII (i.e., time-reversal invariant) can be realized by proximitizing a 2D TI [67–69] with an $s_{\pm}$-wave superconductor [70–72], as sketched in Fig. 1(a). While the bulk has an insulating gap and the edges acquire superconducting gaps, there is a Majorana Kramers pair [73–81] at each corner. To demonstrate this TSC, we not only provide an intuitive edge argument but also derive a novel bulk invariant based on an emergent $\mathcal{C}_4$ symmetry. Moreover, we obtain a general phase diagram and suggest two experimental realizations. Remarkably, our scheme requires neither a π Josephson junction nor a magnetic field, and the superconductor used here is topologically trivial and has a high critical temperature. Therefore, our work establishes a new route for exploring TSCs and Majorana bound states in higher order and at higher temperature [74].

Minimal model.—We first introduce a time-reversal-invariant (TRI) model with two orbitals per site in a square

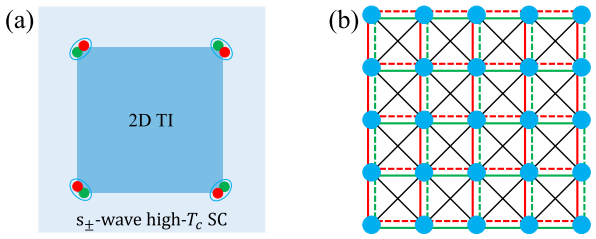

FIG. 1. Schematics of (a) a 2D TI proximitized by a nodeless high-T_c (e.g., Fe-based $s_{\pm}$-wave) superconductor yielding Majorana corner states and (b) a square-lattice model to realize (a). Details in (b) are described below Eq. (1).

lattice, as sketched in Fig. 1(b), to describe a 2D TI proximitized by an $s_\pm$-wave superconductor,

$$H = \left(t\sum_{\langle ij\rangle_x,s} - t\sum_{\langle ij\rangle_y,s} + t_1\sum_{\langle\langle ij\rangle\rangle,s}\right)c^\dagger_{i\mu s}\sigma_z^{\mu\nu}c_{j\nu s} + i\lambda\sum_{\langle ij\rangle}c^\dagger_{i\mu\alpha}(\boldsymbol{s}^{\alpha\beta}\times\hat{\boldsymbol{d}}^{ij})_z\sigma_x^{\mu\nu}c_{j\nu\beta} + \Delta_0\sum_{i,\sigma}c^\dagger_{i\sigma\uparrow}c^\dagger_{i\sigma\downarrow} + \Delta_1\sum_{\langle ij\rangle,\sigma}c^\dagger_{i\sigma\uparrow}c^\dagger_{j\sigma\downarrow} + \text{H.c.}. \quad (1)$$

Here $\boldsymbol{s}$ and $\boldsymbol{\sigma}$ are the Pauli matrices for the spin and orbital spaces, respectively. The t-term is the nearest-neighbor intraorbital hopping; it has opposite signs in the $\hat{x}$ and $\hat{y}$ directions [distinguished by the solid and dashed lines in Fig. 1(b)] and also for the two orbitals [distinguished by the red and green lines in Fig. 1(b)]. The t_1-term is the next-nearest-neighbor intraorbital hopping; it also has opposite signs for the two orbitals. The λ-term arises from the interorbital Rashba spin-orbit coupling; $\boldsymbol{d}^{ij}$ is a vector pointing from site j to site i. Δ_0 and Δ_1 combine to provide an $s_\pm$-wave pairing.

It is more convenient to rewrite Eq. (1) as the following Bogoliubov–de Gennes (BdG) Hamiltonian:

$$\begin{aligned}\mathcal{H}^{\text{BdG}}_{\boldsymbol{k}} &= (h^{\text{TI}}_{\boldsymbol{k}} - \mu)\tau_z + \Delta_{\boldsymbol{k}}\tau_x,\\ h^{\text{TI}}_{\boldsymbol{k}} &= [2t(\cos k_x - \cos k_y) + 4t_1\cos k_x\cos k_y]\sigma_z \\ &\quad + 2\lambda(\sin k_x s_y - \sin k_y s_x)\sigma_x,\\ \Delta_{\boldsymbol{k}} &= \Delta_0 + 2\Delta_1(\cos k_x + \cos k_y),\end{aligned} \quad (2)$$

where μ is the chemical potential and $\boldsymbol{\tau}$ are the Pauli matrices in Nambu particle-hole notation. $\Delta_{\boldsymbol{k}}$ is the $s_\pm$-wave pairing that switches signs between the zone center Γ (0,0) and the zone corner M (π,π) when $|\Delta_0| < 4|\Delta_1|$. The 2D material can acquire such an $s_\pm$-wave pair potential, e.g., when it is proximity coupled to a nodeless Fe-based superconductor [70–72]. Importantly, our model (2) has time-reversal ($\Theta = is_y\mathcal{K}$), particle-hole ($\Xi = s_y\tau_y\mathcal{K}$), and inversion ($\mathcal{P} = \sigma_z$) symmetries. These symmetries can be expressed as follows:

$$\begin{aligned}\Theta\mathcal{H}^{\text{BdG}}(\boldsymbol{k})\Theta^{-1} &= \mathcal{H}^{\text{BdG}}(-\boldsymbol{k}),\\ \Xi\mathcal{H}^{\text{BdG}}(\boldsymbol{k})\Xi^{-1} &= -\mathcal{H}^{\text{BdG}}(-\boldsymbol{k}),\\ \mathcal{P}\mathcal{H}^{\text{BdG}}(\boldsymbol{k})\mathcal{P}^{-1} &= \mathcal{H}^{\text{BdG}}(-\boldsymbol{k}).\end{aligned} \quad (3)$$

The 2D material is described by h^{TI} in Eq. (2) and respects the time-reversal and inversion symmetries in Eq. (3). The spectrum of h^{TI} is generally gapped except when $t_1 = 0$ or $|t| = |t_1|$. Thus, the Fu-Kane criterion [82] based on the eigenvalues of $\mathcal{P}$ at the four TRI momenta can be used to evaluate whether or not the 2D material is a TI. Since h^{TI} is the same at (0, 0) and (π,π), the $\mathbb{Z}_2$ index is determined by the relative band inversion from $(\pi,0)$ to $(0,\pi)$. As listed in Table I, the material is a TI for $|t| > |t_1|$, and a trivial insulator otherwise.

TABLE I. Band inversion at the TRI momenta, the TI $\mathbb{Z}_2$ index of $h^{\text{TI}}_{\boldsymbol{k}}$, and the second-order TSC $\mathbb{Z}_2$ index of $\mathcal{H}^{\text{BdG}}_{\boldsymbol{k}}$ for the cases with $t > 0$ and $\mu = 0$. The cases with $t < 0$ and $\mu = 0$ can be obtained by switching the indices at $(\pi,0)$ and $(0,\pi)$. + and − denote the parity of the number of band inversions.

Condition	(0, 0)	$(\pi,0)$	$(0,\pi)$	(π,π)	$\mathbb{Z}_2$-TI	$\mathbb{Z}_2$-TSC
$t > t_1 > 0$	+	−	+	+	1	1
$t_1 > t > 0$	+	−	−	+	0	0
$t > -t_1 > 0$	−	−	+	−	1	1
$-t_1 > t > 0$	−	+	+	−	0	0

Consider the case in which the 2D TI has only one band inversion at $(\pi,0)$. Figures 2(a) and 2(c) plot the band structures of TI ribbons along the $\hat{x}$ and $\hat{y}$ directions. As anticipated, the $(0\bar{1})$ edge state emerges at $k_x = \pi$, whereas the $(\bar{1}0)$ edge state emerges at $k_y = 0$. When the Fermi energy lies in the bulk gap, the proximity induced $s_\pm$-wave pairing $\Delta_{\boldsymbol{k}}$ can gap out both edge states by breaking the gauge symmetry, as shown in Figs. 2(b) and 2(d) for the $\Delta_0 = 0$ case. For a proximitized TI in a square shape such as that sketched in Fig. 1(a), in spite of the fact that the 2D bulk and the 1D edges are all fully gapped, there are four zero-energy Majorana Kramers pairs—one at each corner,

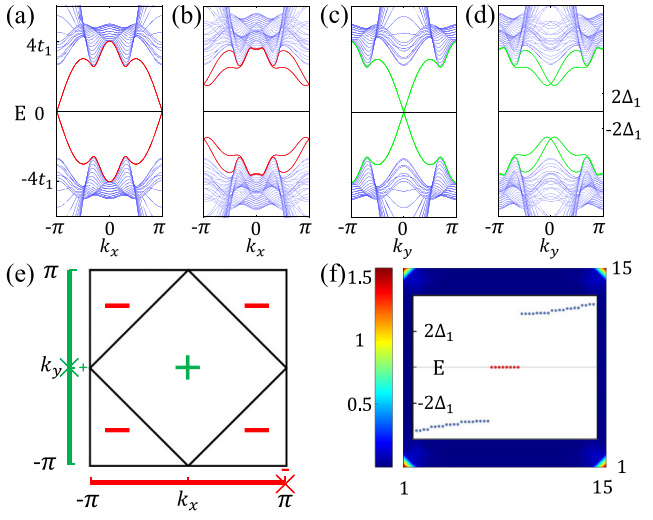

FIG. 2. (a) Band structure of a 2D TI ribbon exhibiting a $(0\bar{1})$ helical edge state at $k_x = \pi$. (b) BdG spectrum of (a) with an $s_\pm$-wave pairing. (c)–(d) Similar to (a)–(b), but exhibiting a $(\bar{1}0)$ helical edge state at $k_y = 0$. (e) Schematic of the $s_\pm$-wave pairing in the bulk BZ and the s-wave pairing of opposite signs acquired by the two edge states. (f) Exact diagonalization revealing the four pairs of Majorana corner states for the 15×15 square size TI. The density plot displays their corner localized probability distribution, and the inset features their symmetry enforced zero energy. We have chosen $t_1 = 1$, $t = 2$, $\lambda = 1.5$, $\Delta_0 = 0$, $\Delta_1 = 0.5$, and $\mu = 0.5$ in all panels.

as exhibited by Fig. 2(f). Evidently, this realizes a second-order TSC in class DIII.

An edge argument can explain the presence of a local Majorana Kramers pair when μ is small, as illustrated in Fig. 2(e). At the $(0\bar{1})$ edge, the helical edge state at $k_x = \pi$ acquires a negative pairing since $\Delta_{\boldsymbol{k}}$ is negative at $k_x = \pi$ for all k_y's. By contrast, at the $(\bar{1}0)$ edge, the helical edge state at $k_y = 0$ acquires a positive pairing since $\Delta_{\boldsymbol{k}}$ is positive at $k_y = 0$ for all k_x's. In light of the topological criterion for 1D TSCs in class DIII [73,74], such a pairing sign reversal leads to the emergence of a boundary Majorana Kramers pair. This argument applies equally to the four corners in Fig. 2(f).

Topological invariant.—The edge argument is intuitive in understanding the second-order TSC, yet the edge-state theory is valid only near the Dirac points. (In fact, a helical edge state cannot be captured by any 1D lattice model.) However, not only can μ be far from the Dirac points but $\Delta_{\boldsymbol{k}}$ also has a strong $\boldsymbol{k}$ dependence across the Brillouin zone (BZ). Thus, it is necessary to establish a topological invariant by using the 2D bulk state.

The bulk model (2) is invariant under the spinful fourfold rotation, accompanied by a gauge transformation that flips the signs of the Δ_1 pairing, the odd-parity orbital on one set of $\sqrt{2}\times\sqrt{2}$ sublattices, and the even-parity orbital on the other set. This *composite*-$\mathcal{C}_4$ symmetry reads

$$\mathcal{C}_4\mathcal{H}^{\mathrm{BdG}}(k_x,k_y)\mathcal{C}_4^{-1} = \mathcal{H}^{\mathrm{BdG}}(\pi-k_y,\pi+k_x), \tag{4}$$

with $\mathcal{C}_4 = \sigma_z\tau_z e^{-is_z\pi/4}$ for $\Delta_0 = 0$. (Note that the *usual*-$\mathcal{C}_4$ symmetry is broken.) Essentially, the four symmetry operators fulfill the following algebra:

$$\begin{aligned} &\Xi^2 = \mathcal{P}^2 = 1, \qquad \Theta^2 = (\mathcal{C}_4)^4 = -1, \\ &[\Theta,\Xi] = [\Xi,\mathcal{P}] = [\mathcal{P},\Theta] = 0, \\ &[\mathcal{C}_4,\Theta] = [\mathcal{C}_4,\mathcal{P}] = 0, \quad \{\mathcal{C}_4,\Xi\} = 0. \end{aligned} \tag{5}$$

Clearly, there are only two TRI momenta in the first BZ that are invariant under the $\mathcal{C}_4$ operation: $(\pi,0)$ and $(0,\pi)$. At these two momenta, all energy states can be labeled by the eigenvalues of $\mathcal{C}_4$

$$\xi_{mn} = e^{i\pi[m+2(1-n)]/4}, \qquad m,n = \pm 1. \tag{6}$$

Physically, m is the eigenvalue of s_z denoting up and down spins of each Kramers doublet, and n is the eigenvalue of τ_z denoting particle and hole states in the BdG formalism. Thus, ξ_{mn} transforms as follows:

$$\Theta\colon\ (m,n)\to(-m,n), \qquad \Xi\colon\ (m,n)\to(-m,-n). \tag{7}$$

Evidently, states with $\mathcal{C}_4$ eigenvalues $e^{\pm i\pi/4}$ (or $e^{\pm i3\pi/4}$) form $n = 1$ (or $n = -1$) Kramers doublets, and these two groups are related by the particle-hole symmetry.

We now use the eigenvalues of $\mathcal{P}$ to establish the bulk topological invariant, built upon the algebra in Eq. (5). (i) As $\mathcal{P}$ commutes with both Θ and $\mathcal{C}_4$, the two states in each Kramers doublet ($m = \pm 1$) must share the same $\mathcal{P}$ eigenvalue. (ii) In an anomaly-free lattice model, all of the particle ($n = 1$) or hole ($n = -1$) states must have an even number of Kramers doublets with $\mathcal{P}$ eigenvalue -1 at the two $\mathcal{C}_4$ invariant momenta. (iii) As $\mathcal{P}$ commutes with Ξ, the particle and hole states of opposite energies must have the same number of Kramers doublets with $\mathcal{P}$ eigenvalue -1 at each $\mathcal{C}_4$ invariant momentum.

Therefore, there is a $\mathbb{Z}_2$ topological invariant for the studied second-order TSC: the parity of the number of negative-energy Kramers doublets with $\mathcal{C}_4$ eigenvalues $e^{\pm i\pi/4}$ (i.e., the particle states) and $\mathcal{P}$ eigenvalue -1 at the two $\mathcal{C}_4$ invariant momenta. The odd (or even) parity determines the presence (or absence) of the four pairs of symmetry-protected Majorana corner states. This $\mathbb{Z}_2$ criterion can be applied to any square-shaped case (e.g., Fig. 2) regardless of orientation, as long as it respects the $\mathcal{C}_4$ symmetry. Since the energy reference is the Fermi energy and the pairing vanishes at the $\mathcal{C}_4$ invariant momenta, the $\mathbb{Z}_2$ criterion is reduced to the parity of the number of band inversions at $(\pi,0)$ and $(0,\pi)$ when the Fermi energy is in the band gap of h^{TI}. This is consistent with our numerical results summarized in Table I. We point out that the $\mathbb{Z}_2$ invariant can alternatively be proved by a bulk-boundary correspondence [83].

Phase diagram.—More generally, the protection of a local Majorana Kramers pair requires only time-reversal and particle-hole symmetries. The former dictates the Kramers degeneracy, and the latter pins the Kramers pair to zero energy. Consequently, the Majorana corner states in Fig. 2(f) is robust against the breaking of inversion and composite-$\mathcal{C}_4$ symmetries, e.g., by a nonzero Δ_0, a tilted edge orientation, or nonopposite hopping amplitudes, as long as the perturbation does not close the energy gap or hybridize Majorana bound states at different corners.

Figure 3(a) shows the phase diagram of our model (2) versus Δ_0 and μ for a case in which the 2D TI has only one band inversion at $(\pi,0)$. Since the phase diagram is symmetric around $\Delta_0 = 0$ and $\mu = 0$, we focus on the case with $\Delta_0 \geq 0$ and $\mu \geq 0$. At $\Delta_0 = 0$, the $\mathcal{C}_4$ symmetry is intact, and the established topological criterion is applicable. When μ lies in the band gap of the TI, the phase is topologically nontrivial, as there is one negative-energy Kramers doublet with $\mathcal{C}_4$ eigenvalues $e^{\pm i\pi/4}$ and $\mathcal{P}$ eigenvalue -1 at $(\pi,0)$, whereas none at $(0,\pi)$—the total parity is odd. When μ crosses the conduction band, if the Fermi surface and the nodal lines of $\Delta_{\boldsymbol{k}}$ intersect, the phase becomes nodal. When μ is beyond the entire conduction band, the phase must be trivial; at each $\mathcal{C}_4$ invariant momentum, the one Kramers doublet with $\mathcal{C}_4$ eigenvalues $e^{\pm i\pi/4}$ and $\mathcal{P}$ eigenvalue -1 is below the Fermi energy—the total parity is even.

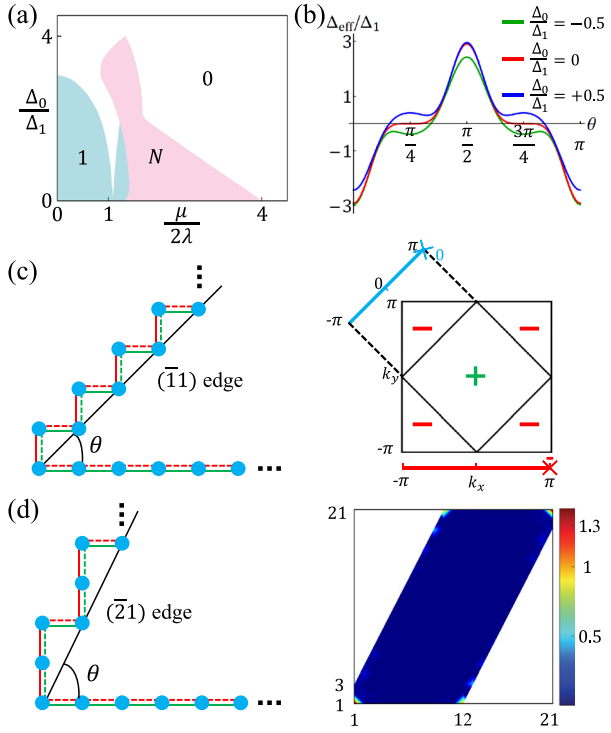

FIG. 3. (a) Phase diagram of the second-order TSC versus Δ_0 and μ, distinguishing the topological (1), trivial (0), and nodal (N) phases. (b) Effective pairing $\Delta_{\rm eff}$ acquired by the edge state versus the tilted edge orientation θ. (c) Schematic of $\Delta_{\rm eff} = 0$ for the $(\bar{1}1)$ edge state. (d) Spatial probability distribution revealing the four pairs of Majorana corner states for the 11×21 parallelogram size TI. We have chosen $t_1 = 1$, $t = 2$, $\lambda = 1.5$, $\Delta_1 = 1$ in (a)–(d), $\mu = 0$ in (b)–(d), and $\Delta_0 = 0$ in (c) and (d).

As Δ_0 increases from zero, the topological character remains unless there is a gap closure in the 2D bulk or at a 1D edge, as shown in Fig. 3(a). When Δ_0 is above a threshold $\lesssim 4\Delta_1$, the induced pair potential has a uniform sign at all edges, and the edge superconductivity must be trivial without the sign reversal [73,74]. As μ increases from zero, the $(0\bar{1})$-edge-state Fermi points move from $k_x = \pi$ to $k_x = 0$, whereas the $(\bar{1}0)$-edge-state Fermi points move from $k_y = 0$ to $k_y = \pi$. For $\Delta_0 = 0$, the switch occurs at $k^c = \pi/2$ of both edges, resulting in an accidental gap closure near $\mu = 2\lambda \sin k^c$. For $\Delta_0 > 0$, however, $k_x^c \neq k_y^c$, and the edge gap closes and reopens twice near $\mu_{x,y} = 2\lambda \sin k_{x,y}^c$; each reverses the pairing sign of one of two edge states. As a result, the phase is topologically nontrivial before and after the two gap closures but trivial in between. This explains the presence of two topological domes in Fig. 3(a). In addition, the larger the value of Δ_0, the smaller the nodal lines of $\Delta_{\boldsymbol{k}}$, giving rise to the shrinking of the nodal regime in the phase diagram with increasing Δ_0.

Now we reveal the stability of Majorana corner states against the edge orientations of 2D TI. Without loss of generality, we study the $\mu = 0$ case for the corner connecting the $(0\bar{1})$ edge and the edge with a tilted angle of θ from it. Since the $(0\bar{1})$ edge state acquires a negative pairing, the positive or negative sign of $\Delta_{\rm eff}$, i.e., the pairing acquired by the tilted edge state, determines whether the phase is topologically nontrivial or trivial [73,74]. Figure 3(b) displays $\Delta_{\rm eff}$ versus θ, as extracted from our numerical calculations. For $\Delta_0 = 0$, the two critical points occur at $\theta = \pi/4$ and $3\pi/4$, where $\Delta_{\rm eff}$ vanishes, as illustrated in Fig. 3(c). Figure 3(d) sketches a parallelogram-shaped TI with $\theta = \arctan 2$ and features the four pairs of Majorana corner states, demonstrating that this case is still a second-order TSC. Generally, for a positive (or negative) Δ_0, the topological regime is enlarged (or suppressed).

Experiment and discussion.—There are two limits for the proximity effects. One arises from strong chemical bonding between superconducting and normal materials. Prime examples are the graphene-MoRe *lateral* junction with strong p_z-d hybridization [84] and the intrinsic proximity effect in $FeTe_{1-x}Se_x$ ($x = 0.45$) [65,66]. The other one arises from weak electron tunneling between superconducting and normal states [85]. This includes our proposed setup and the observed proximity effects in graphene–yttrium barium copper oxide and TI–bismuth strontium calcium copper oxide systems [86,87]; in these *vertical* junctions, tunnelings occur between p (also the case for PbS and WTe_2 below) and d orbitals. Note that a vertical junction breaks mirror symmetry and that the required tunneling is generally allowed. In our case, to maintain the phase coherence of $\boldsymbol{k}$-dependent pairing, a lattice match between the TI and superconductor is desired. IV-VI monolayers have been identified as tunable 2D TIs [67–69], with independently controllable band inversions at $(\pi, 0)$ and $(0, \pi)$ [69]. The monolayer PbS has a square-lattice constant of 4.03 Å [69], comparable to 3.95–4.05 Å of iron pnictides [72]. A proximity effect has already been observed in PbS [88]. Thus, the PbS–iron pnictide vertical junction can be a candidate system to explore the proposed second-order TSC.

Although we focus on the scenario in which the 2D TI has one band inversion at $(\pi, 0)$, Majorana corner states can exist in other scenarios. (i) Consider a TI with one band inversion at (0,0) or (π, π). For a $d_{x^2-y^2}$-wave pairing (if nodeless), very similar physics is anticipated; for an $s_\pm$-wave pairing, Majorana corner states are possible only if the TI breaks the rotational symmetry. (ii) Consider a TI with two band inversions, e.g., at (0,0) and $(\pi, 0)$. For either aforementioned pairing, both the (01) and $(0\bar{1})$ edges have dual helical edge states at $k_x = 0, \pi$ and may become TSCs, whereas both the (10) and $(\bar{1}0)$ edges are trivial. Interesting, monolayer WTe_2 as a TI up to 100 K [89,90] has one band inversion at (0, 0) and may be exploited for scenario (i). We stress that the usual-$\mathcal{C}_4$ symmetry must be broken in all three models; otherwise, the four edges would have the same sign in pair potential yielding a trivial phase [73,74].

As critical advantages, our scheme requires neither a π Josephson junction nor a magnetic field, and the superconductor can enjoy a critical temperature as high as 56 K in $Sr_{0.5}Sm_{0.5}FeAsF$ [91]. In probing the Majorana corner states, because of the Kramers degeneracy, the zero-bias tunneling conductance is anticipated to be $4e^2/h$ [74] at each corner when the TSC is grounded. For a Josephson junction with two corners in contact, the two Majorana Kramers pairs are expected to produce a 4π periodic fractional Josephson effect [92]. Finally, we point out that our second-order Majorana corner states should exhibit non-Abelian braiding statistics [92–95] and, under interactions, should give rise to exotic Kondo effects [96], an 8π Josephson effect [6], and higher-order $\mathbb{Z}_4$ parafermions [6,97,98].

This work was supported by ARO under Grant No. W911NF-18-1-0416 (Q. W. and F. Z.), UTD research enhancement funds (Q. W. and F. Z.), NSF under Grant No. DMR-1653769 (Y.-M. L.), NSFC under Grant No. 11774028 (C.-C. L.), and BIT basic research funds No. 2017CX01018 (C.-C. L.).

Q. W. and C.-C. L. contributed equally to this work.

Note added.—Recently, we became aware of two complementary studies [99,100]. Reference [99] is based on an edge theory of a different model without establishing a bulk topological invariant. Reference [100] focuses on completely different and more exotic pairing symmetries.

*zhang@utdallas.edu

[1] J. E. Moore, Nature (London) **464**, 194 (2010).
[2] M. Z. Hasan and C. L. Kane, Rev. Mod. Phys. **82**, 3045 (2010).
[3] X.-L. Qi and S.-C. Zhang, Rev. Mod. Phys. **83**, 1057 (2011).
[4] C.-K. Chiu, J. C. Y. Teo, A. P. Schnyder, and S. Ryu, Rev. Mod. Phys., **88**, 035005 (2016).
[5] L. Fu and C. L. Kane, Phys. Rev. Lett. **100**, 096407 (2008).
[6] F. Zhang and C. L. Kane, Phys. Rev. Lett. **113**, 036401 (2014).
[7] R. Yu, W. Zhang, H. Zhang, S. Zhang, X. Dai, and Z. Fang, Science **329**, 61 (2010).
[8] F. Zhang, C. L. Kane, and E. J. Mele, Phys. Rev. Lett. **110**, 046404 (2013).
[9] W. A. Benalcazar, B. A. Bernevig, and T. L. Hughes, Science **357**, 61 (2017).
[10] M. Serra-Garcia, V. Peri, R. Süsstrunk, O. R. Bilal, T. Larsen, L. G. Villanueva, and S. D. Huber, Nature (London) **555**, 342 (2018).
[11] S. A. Parameswaran and Y. Wan, Physics **10**, 132 (2017).
[12] W. A. Benalcazar, B. A. Bernevig, and T. L. Hughes, Phys. Rev. B **96**, 245115 (2017).
[13] J. Langbehn, Y. Peng, L. Trifunovic, F. von Oppen, and P. W. Brouwer, Phys. Rev. Lett. **119**, 246401 (2017).
[14] Z. Song, Z. Fang, and C. Fang, Phys. Rev. Lett. **119**, 246402 (2017).
[15] B. J. Wieder, B. Bradlyn, Z. Wang, J. Cano, Y. Kim, H. D. Kim, A. M. Rappe, C. L. Kane, and B. A. Bernevig, Science **361**, 246 (2018).Z. Wang, B. J. Wieder, J. Li, B. Yan, and B. A. Bernevig, arXiv:1806.11116.
[16] F. Schindler, A. M. Cook, M. G. Vergniory, Z. Wang, S. S. P. Parkin, B. A. Bernevig, and T. Neupert, Sci. Adv. **4**, eaat0346 (2018).
[17] C. Fang and L. Fu, arXiv:1709.01929.
[18] L. Li, H. H. Yap, M. A. N. Araujo, and J. Gong, Phys. Rev. B **96**, 235424 (2017).
[19] M. Ezawa, Phys. Rev. Lett. **120**, 026801 (2018).
[20] M. Ezawa, Phys. Rev. B **98**, 045125 (2018); **97**, 155305 (2018); **97**, 241402(R) (2018).
[21] F. Schindler, Z. Wang, M. G. Vergniory, A. M. Cook, A. Murani, S. Sengupta, A. Y. Kasumov, R. Deblock, S. Jeon, I. Drozdov, H. Bouchiat, S. Gueron, A. Yazdani, B. A. Bernevig, and T. Neupert, Nat. Phys. **14**, 918 (2018).
[22] E. Khalaf, Phys. Rev. B **97**, 205136 (2018); M. Geier, L. Trifunovic, M. Hoskam, and P. W. Brouwer, Phys. Rev. B **97**, 205135 (2018); X. Zhu, Phys. Rev. B **97**, 205134 (2018).
[23] N. Read and D. Green, Phys. Rev. B **61**, 10267 (2000).
[24] A. Y. Kitaev, Phys. Usp. **44**, 131 (2001).
[25] D. A. Ivanov, Phys. Rev. Lett. **86**, 268 (2001).
[26] C. Nayak, S. H. Simon, A. Stern, M. Freedman, and S. Das Sarma, Rev. Mod. Phys. **80**, 1083 (2008).
[27] L. Fu and C. L. Kane, Phys. Rev. B **79**, 161408(R) (2009).
[28] K. T. Law, P. A. Lee, and T. K. Ng, Phys. Rev. Lett. **103**, 237001 (2009).
[29] J. Nilsson, A. R. Akhmerov, and C. W. J. Beenakker, Phys. Rev. Lett. **101**, 120403 (2008).
[30] J. D. Sau, R. M. Lutchyn, S. Tewari, and S. Das Sarma, Phys. Rev. Lett. **104**, 040502 (2010).
[31] J. Alicea, Phys. Rev. B **81**, 125318 (2010).
[32] R. M. Lutchyn, J. D. Sau, and S. Das Sarma, Phys. Rev. Lett. **105**, 077001 (2010).
[33] Y. Oreg, G. Refael, and F. von Oppen, Phys. Rev. Lett. **105**, 177002 (2010).
[34] J. Alicea, Rep. Prog. Phys. **75**, 076501 (2012).
[35] C. Beenakker, Annu. Rev. Condens. Matter Phys. **4**, 113 (2013).
[36] T. D. Stanescu and S. Tewari, J. Phys. Condens. Matter **25**, 233201 (2013).
[37] S. R. Elliott and M. Franz, Rev. Mod. Phys. **87**, 137 (2015).
[38] C. W. J. Beenakker, Rev. Mod. Phys. **87**, 1037 (2015).
[39] R. Aguado, Riv. Nuovo Cimento Soc. Ital. Fis. **40**, 523 (2017).
[40] M. Hell, M. Leijnse, and K. Flensberg, Phys. Rev. Lett. **118**, 107701 (2017).
[41] J. Cayao, P. San-Jose, A. M. Black-Schaffer, R. Aguado, and E. Prada, Phys. Rev. B **96**, 205425 (2017).
[42] V. Mourik, K. Zuo, S. M. Frolov, S. R. Plissard, E. P. A. M. Bakkers, and L. P. Kouwenhoven, Science **336**, 1003 (2012).
[43] L. P. Rokhinson, X. Liu, and J. K. Furdyna, Nat. Phys. **8**, 795 (2012).

[44] A. Das, Y. Ronen, Y. Most, Y. Oreg, M. Heiblum, and H. Shtrikman, Nat. Phys. **8**, 887 (2012).
[45] M. T. Deng, C. L. Yu, G. Y. Huang, M. Larsson, P. Caroff, and H. Q. Xu, Nano Lett. **12**, 6414 (2012).
[46] A. D. K. Finck, D. J. Van Harlingen, P. K. Mohseni, K. Jung, and X. Li, Phys. Rev. Lett. **110**, 126406 (2013).
[47] H. O. H. Churchill, V. Fatemi, K. Grove-Rasmussen, M. T. Deng, P. Caroff, H. Q. Xu, and C. M. Marcus, Phys. Rev. B **87**, 241401 (2013).
[48] S. Nadj-Perge, I. K. Drozdov, J. Li, H. Chen, S. Jeon, J. Seo, A. H. MacDonald, B. A. Bernevig, and A. Yazdani, Science **346**, 602 (2014).
[49] W. Chang, S. M. Albrecht, T. S. Jespersen, F. Kuemmeth, P. Krogstrup, J. Nygård, and C. M. Marcus, Nat. Nanotechnol. **10**, 232 (2015).
[50] S. M. Albrecht, A. P. Higginbotham, M. Madsen, F. Kuemmeth, T. S. Jespersen, J. Nygard, P. Krogstrup, and C. M. Marcus, Nature (London) **531**, 206 (2016).
[51] M. T. Deng, S. Vaitiekėnas, E. B. Hansen, J. Danon, M. Leijnse, K. Flensberg, J. Nygård, P. Krogstrup, and C. M. Marcus, Science **354**, 1557 (2016).
[52] M. Kjaergaard, F. Nichele, H. J. Suominen, M. P. Nowak, M. Wimmer, A. R. Akhmerov, J. A. Folk, K. Flensberg, J. Shabani, C. J. Palmstrøm, and C. M. Marcus, Nat. Commun. **7**, 12841 (2016).
[53] J. Wiedenmann, E. Bocquillon, R. S. Deacon, S. Hartinger, O. Herrmann, T. M. Klapwijk, L. Maier, C. Ames, C. Brüne, C. Gould, A. Oiwa, K. Ishibashi, S. Tarucha, H. Buhmann, and L. W. Molenkamp, Nat. Commun. **7**, 10303 (2016).
[54] J. Chen, P. Yu, J. Stenger, M. Hocevar, D. Car, S. R. Plissard, E. P. A. M. Bakkers, T. D. Stanescu, and S. M. Frolov, Sci. Adv. **3**, e1701476 (2017).
[55] H. J. Suominen, M. Kjaergaard, A. R. Hamilton, J. Shabani, C. J. Palmstrøm, C. M. Marcus, and F. Nichele, Phys. Rev. Lett. **119**, 176805 (2017).
[56] F. Nichele, A. C. C. Drachmann, A. M. Whiticar, E. C. T. O'Farrell, H. J. Suominen, A. Fornieri, T. Wang, G. C. Gardner, C. Thomas, A. T. Hatke, P. Krogstrup, M. J. Manfra, K. Flensberg, and C. M. Marcus, Phys. Rev. Lett. **119**, 136803 (2017).
[57] E. Bocquillon, R. S. Deacon, J. Wiedenmann, P. Leubner, T. M. Klapwijk, C. Brüne, K. Ishibashi, H. Buhmann, and L. W. Molenkamp, Nat. Nanotechnol. **12**, 137 (2017).
[58] M. Banerjee, M. Heiblum, A. Rosenblatt, Y. Oreg, D. E. Feldman, A. Stern, and V. Umansky, Nature (London) **545**, 75 (2017).
[59] Q. L. He *et al.*, Science **357**, 294 (2017).
[60] H. Zhang *et al.*, Nature (London) **556**, 74 (2018).
[61] W. Yu, W. Pan, D. L. Medlin, M. A. Rodriguez, S. R. Lee, Z.-Q. Bao, and F. Zhang, Phys. Rev. Lett. **120**, 177704 (2018).
[62] C. Li, J. C. de Boer, B. de Ronde, S. V. Ramankutty, E. van Heumen, Y. Huang, A. de Visser, A. A. Golubov, M. S. Golden, and A. Brinkman, Nat. Mater. **17**, 875 (2018).
[63] D. Laroche, D. Bouman, D. J. van Woerkom, A. Proutski, C. Murthy, D. I. Pikulin, C. Nayak, R. J. J. van Gulik, J. Nygård, P. Krogstrup, L. P. Kouwenhoven, and A. Geresdi, arXiv:1712.08459.
[64] F. Zhang and W. Pan, Nat. Mater. **17**, 851 (2018).
[65] P. Zhang, K. Yaji, T. Hashimoto, Y. Ota, T. Kondo, K. Okazaki, Z. Wang, J. Wen, G. D. Gu, H. Ding, and S. Shin, Science **360**, 182 (2018).
[66] D. Wang, L. Kong, P. Fan, H. Chen, S. Zhu, W. Liu, L. Cao, Y. Sun, S. Du, J. Schneeloch, R. Zhong, G. Gu, L. Fu, H. Ding, and H. J. Gao, Science **362**, eaao1797 (2018).
[67] J. W. Liu, X. F. Qian, and L. Fu, Nano Lett. **15**, 2657 (2015).
[68] E. O. Wrasse and T. M. Schmidt, Nano Lett. **14**, 5717 (2014).
[69] W. Wan, Y. Yao, L. Sun, C.-C. Liu, and F. Zhang, Adv. Mater. **29**, 1604788 (2017).
[70] I. I. Mazin, Nature (London) **464**, 183 (2010).
[71] I. Bozovic and C. Ahn, Nat. Phys. **10**, 892 (2014).
[72] P. Dai, Rev. Mod. Phys. **87**, 855 (2015).
[73] X.-L. Qi, T. L. Hughes, and S.-C. Zhang, Phys. Rev. B **81**, 134508 (2010).
[74] F. Zhang, C. L. Kane, and E. J. Mele, Phys. Rev. Lett. **111**, 056402 (2013); **111**, 056403 (2013).
[75] C. L. M. Wong and K. T. Law, Phys. Rev. B **86**, 184516 (2012).
[76] S. Nakosai, J. C. Budich, Y. Tanaka, B. Trauzettel, and N. Nagaosa, Phys. Rev. Lett. **110**, 117002 (2013).
[77] A. Keselman, L. Fu, A. Stern, and E. Berg, Phys. Rev. Lett. **111**, 116402 (2013).
[78] E. Gaidamauskas, J. Paaske, and K. Flensberg, Phys. Rev. Lett. **112**, 126402 (2014).
[79] J. Klinovaja, A. Yacoby, and D. Loss, Phys. Rev. B **90**, 155447 (2014).
[80] A. Haim, A. Keselman, E. Berg, and Y. Oreg, Phys. Rev. B **89**, 220504 (2014).
[81] C. Schrade, A. A. Zyuzin, J. Klinovaja, and D. Loss, Phys. Rev. Lett. **115**, 237001 (2015).
[82] L. Fu and C. L. Kane, Phys. Rev. B **76**, 045302 (2007).
[83] See Supplemental Material at http://link.aps.org/supplemental/10.1103/PhysRevLett.121.186801 for the alternative proof of our novel $\mathbb{Z}_2$ invariant that classifies our second-order TSCs.
[84] F. Amet, C. T. Ke, I. V. Borzenets, J. Wang, K. Watanabe, T. Taniguchi, R. S. Deacon, M. Yamamoto, Y. Bomze, S. Tarucha, and G. Finkelstein, Science **352**, 966 (2016).
[85] W. L. McMillan, Phys. Rev. **175**, 537 (1968).
[86] D. Perconte, F. A. Cuellar, C. Moreau-Luchaire, M. Piquemal-Banci, R. Galceran, P. R. Kidambi, M. Martin, S. Hofmann, R. Bernard, B. Dlubak, P. Seneor, and J. E. Villegas, Nat. Phys. **14**, 25 (2018).
[87] P. Zareapour, A. Hayat, S. Zhao, M. Kreshchuk, A. Jain, D. C. Kwok, N. Lee, S.-W. Cheong, Z. Xu, A. Yang, G. D. Gu, S. Jia, R. J. Cava, and K. S. Burch, Nat. Commun. **3**, 1056 (2012).
[88] B. Kim, H. Kim, Y. Yang, X. Peng, D. Yu, and Y. Doh, ACS Nano **11**, 221 (2017).
[89] X. Qian, J. Liu, L. Fu, and J. Li, Science **346**, 1344 (2014).
[90] S. Wu, V. Fatemi, Q. D. Gibson, K. Watanabe, T. Taniguchi, R. J. Cava, and P. Jarillo-Herrero, Science **359**, 76 (2018).
[91] G. Wu, Y. L. Xie, H. Chen, M. Zhong, R. H. Liu, B. C. Shi, Q. J. Li, X. F. Wang, T. Wu, Y. J. Yan, J. J. Ying, and X. H. Chen, J. Phys. Condens. Matter **21**, 142203 (2009).
[92] F. Zhang and C. L. Kane, Phys. Rev. B **90**, 020501(R) (2014).

[93] X.-J. Liu, C. L. M. Wong, and K. T. Law, Phys. Rev. X **4**, 021018 (2014).
[94] K. Wölms, A. Stern, and K. Flensberg, Phys. Rev. B **93**, 045417 (2016).
[95] C. Schrade and L. Fu, arXiv:1807.06620.
[96] Z.-q. Bao and F. Zhang, Phys. Rev. Lett. **119**, 187701 (2017).
[97] J. Alicea and A. Stern, Phys. Scr. T **T164**, 014006 (2015).
[98] J. Alicea and P. Fendley, Annu. Rev. Condens. Matter Phys. **7**, 119 (2016).
[99] Z. Yan, F. Song, and Z. Wang, arXiv:1803.08545.
[100] Y. Wang, M. Lin, and T. L. Hughes, arXiv:1804.01531.